Nano-Structures & Nano-Objects 14 (2018) 84–91

Contents lists available at ScienceDirect

Nano-Structures & Nano-Objects

journal homepage: www.elsevier.com/locate/nanoso

# Ferrimagnetism in cobalt ferrite ($CoFe_2O_4$) nanoparticles

B. Jansi Rani [a], M. Ravina [a], B. Saravanakumar [b], G. Ravi [a], V. Ganesh [c], S. Ravichandran [d], R. Yuvakkumar [a,*]

[a] Nanomaterials Laboratory, Department of Physics, Alagappa University, Karaikudi 630 003, Tamil Nadu, India
[b] Department of Organic Materials & Fiber Engineering, Chonbuk National University, Jeonju 561 756, South Korea
[c] Electrodics and Electrocatalysis (EEC) Division, CSIR–Central Electrochemical Research Institute (CSIR–CECRI), Karaikudi 630003, Tamil Nadu, India
[d] Electro Inorganic Division, CSIR–Central Electrochemical Research Institute (CSIR–CECRI), Karaikudi, Tamil Nadu 630003, India

## GRAPHICAL ABSTRACT

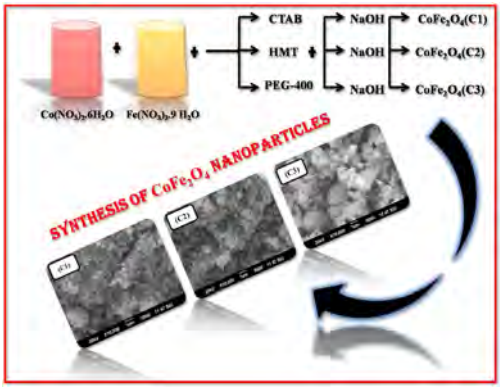


## ARTICLE INFO

*Article history:*
Received 2 August 2017
Received in revised form 23 January 2018
Accepted 31 January 2018

*Keywords:*
Cubic
$CoFe_2O_4$
VSM
Ferrimagnetic

## ABSTRACT

Ferrimagnetic cobalt ferrite ($CoFe_2O_4$) nanoparticles were synthesized by employing co-precipitation method. Product physico-chemical and magnetic properties with respect to cetyl trimethylammonium bromide (CTAB), hexamethylenetetramine (HMT) and polyethylene glycol (PEG-400) surfactants were investigated. XRD pattern and Raman characteristic active modes revealed the cubic cobalt ferrite structure formation. SEM images explored spherical shaped product with different particle size. Identified strong PL emission peaks confirmed the product quality. IR metal oxygen vibration at 615 and 426 $cm^{-1}$ revealed tetrahedral and octahedral site of cobalt ferrite system. Product electrochemical behavior was found to be size dependent and high specific capacitance was observed using CTAB. Room temperature ferrimagnetic behavior was confirmed through VSM studies. High saturation value as 66 emu/g was found using PEG. Particles with larger crystallite and particle size exhibited improved magnetic behavior.



## 1. Introduction

The ferrite physical and chemical properties grasp the researcher's interest to carry out research over a deep insight of analyzing the different ferrite magnetic, electric and opto-electric properties [1–5]. Nano-sized spinel ferrites have been focused due to its smaller particle size and narrow size distribution with larger surface area [1]. Nano-sized cobalt ferrite ($CoFe_2O_4$) filled up the major applications due to its unusual properties like magnetocrystalline high anisotropy ($1.8–3 \times 10^5$ J/$m^3$ at 300 K), good coercivity and enhanced magnetization [2]. Separately, cobalt

* Corresponding author.
*E-mail address:* yuvakkumarr@alagappauniversity.ac.in (R. Yuvakkumar).

https://doi.org/10.1016/j.nanoso.2018.01.012
2352-507X/

oxide and iron oxide are also attracted for their unique properties and low cost [3,4]. Numerous techniques such as heat treatment, chemical substitution and sudden cooling etc. has been adopted to tune cobalt ferrite properties [5,6]. Generally, in bulk cobalt ferrite inverse spinel structure, $Co^{2+}$ ions preferred octahedral B site and $Fe^{3+}$ ions preferred tetrahedral A site of ferrite system. The cations distribution in ferrite system made the respective ferrite nanoparticles being significant in their unique properties for advanced applications. The ferrite magnetic property is directly depending on cations type and distribution in octahedral and tetrahedral sites and vice versa. The magnetic ferrite electron spins are arranged parallel within the crystal lattice site and anti-parallel between two sublattice sites whiles the net magnetization is the difference between two sites. The cobalt ferrite spinel structure is a hopeful phase material for magneto-sensitive systems [7], magnetic resonance imaging (MRI), tissue imaging and other environmental friendly applications [8]. Due to its high mechanical strength and wear anisotropy, it could be tied to the active materials in ferrofluids, microwave devices and adsorption applications [9]. The hierarchical, unusual and novel morphology nanoferrites such as nanoparticles, nanorods, nanocubes, nanobelt and nanoflowers help to adapt the corresponding material for future generation potential applications [10,11]. Several methods have been developed to synthesize nanoferrites including hydrothermal, sol–gel, ball milling, chemical reduction, microwave synthesis, mechanical alloying and co-precipitation etc. Among these methods, co-precipitation method has less toxic and fast and high yield synthesis method [12,13].

Gabal and his co-workers synthesized Zn-substituted $CoFe_2O_4$ via sucrose assisted combustion route and investigated the electromagnetic properties [14]. Pourgolmohammad and his team reported the effect of starting solution acidity on the characteristics of $CoFe_2O_4$ powders prepared by solution combustion synthesis method [15]. Fatemeh Shams and his research group statistically approached $CoFe_2O_4$ nanoparticles to optimize their characteristics using the response surface methodology [16]. Seema Joshi and her colleague worked on analyzing the effect of $Gd^{3+}$ substitution on structural, magnetic, dielectric and optical properties of nanocrystalline $CoFe_2O_4$ [17]. Nagarajan Kannapiran and his group synthesized Poly(*o*-phenylenediamine)/$NiCoFe_2O_4$ nanocomposites and reported its characterization and the magneto-dielectric properties in details [18]. Mikio Kishimoto and his squad synthesized the FeCo particles through co-precipitation route using flux treatment for particle growth and examined the reduction property in hydrogen gas [19]. Kashif Ali and his coworkers synthesized $CuFe_2O_4/MnO_2$ nanocomposites for investigating its magnetic and dielectric properties successfully [20]. Bhowmik and Sinha jointly studied the improvement of room temperature electric polarization and ferrimagnetic properties of $Co_{1.25}Fe_{1.75}O_4$ ferrite by heat treatment [21]. Vijayasundaram and his team investigated chemically synthesized phase-pure nanoparticles and examine the role of influencing agents on the product purity [22]. Chaitali Dey and his research group reported the improved and efficient drug delivery system by hyperthermia treatment using magnetic cubic cobalt ferrite nanoparticles [23]. Chunming Yang and his team mates synthesized novel rare earth ions doped polyaniline/cobalt ferrite nanocomposites via a novel coordination-oxidative polymerization-hydrothermal route and investigated its microwave-absorbing properties [24]. In the present study, preparation of cobalt ferrite ($CoFe_2O_4$) nanoparticles employing simple co-precipitation route using different surfactants such as CTAB, HMT and PEG-400 has been explored. The surfactants effect on vital role in physico-chemical and magnetic properties of synthesized cobalt ferrite nanoparticles have been studied.

## 2. Materials and methods

Cobalt nitrate hexahydrate [$Co(NO_3)_2 \cdot 6H_2O$], ferric nitrate nonahydrate [$Fe(NO_3)_3 \cdot 9H_2O$], sodium hydroxide (NaOH), cetyl trimethylammonium bromide (CTAB), hexamethylenetetramine (HMT) and polyethylene glycol (PEG-400) were purchased from Sigma Aldrich. Wet chemical co-precipitation method was adapted to synthesize cobalt ferrite ($CoFe_2O_4$) nanoparticles. At first, 1 M (mol/L) $Co(NO_3)_2 \cdot 6H_2O$ and 2 M (mol/L) $Fe(NO_3)_3 \cdot 9H_2O$ were mixed together gradually under magnetic stirring and named as solution A. Then, 1 M (mol/L) CTAB was dissolved in 10 ml of deionized water and added slowly into the solution A. This solution was continued in stirring for about 10 min without any other disturbances and named as solution B. 20 M (mol/L) NaOH alkaline solution was poured into solution B as precipitating agent. The pale brown color solution was turned into dark brown color with particles indicated the successful reaction. The particles were washed with ethanol and water and centrifuged and dried at 100 °C overnight. The same procedure was followed by changing the surfactants as HMT and PEG-400. These dried powders were calcinated at 800 °C for 2 h and the final product was named as C1, C2 and C3 respectively and characterized comprehensively employing standard techniques. The product electrochemical behavior and the specific capacitance were examined by employing cyclic voltammeter (CV) study. The synthesized cobalt ferrite using various surfactants such as CTAB, HMT and PEG was chosen as active material. Initially 70% of active material, 20% of conducting agent (activated carbon) and 10% of binder (polyvinylidene hexafluoride-PVDF) were mixed together homogeneously with the help of N-methyl 2 pyrrolidinone solvent. This consistent mixture was layered on the low cost graphite sheet ($1 \times 1$ cm) and dried in hot air oven for 14 h at 120 °C. Finally, the active material coated dried graphite sheet was adapted as working electrode in CV set-up. $Ag/AgCl_2$ was used as reference electrode, platinum wire was used as counter electrode and 1 M of NaOH was taken as electrolyte solution in the CV set-up of CH electrochemical workstation. By the formula and the area of CV curve, the specific capacitance value of respective material was calculated. The potential window was limited as −2.0 V to 1.0 V at various scan rates 15, 30, 45 and 60 respectively.

## 3. Results and discussion

Magnetic cobalt ferrite ($CoFe_2O_4$) nanoparticles are prolifically synthesized by employing wet chemical route with different surfactants such as CTAB, HMT and PEG-400 respectively. During synthesis, CTAB addition leads negative sides of precursor solution to move towards positive heads of CTAB and results lesser coalescence. The dissolved hexamine (HMT) in water produces continuous hydroxide ($OH^-$) ions to the precursor solution and abruptly changes the solution pH. The produced $OH^-$ ions formed micelles layer around the cobalt ferrite hydroxide which leads to compact morphology of spherical shape products with lesser agglomeration. PEG-400 acted as a linking agent and yield larger size particles with uneven diameter and reveals sweeping change in the particle morphology. The advantages of synthesis methods in the present work for competitive products with other works reveals that one can synthesis highly dispersed and diverse morphology of cobalt ferrite nanoparticles when the influencing parameters such as CTAB, HMT and PEG-400 surfactant and the wet chemical synthesis conditions is optimized. The co-precipitation method is one of the simple, less toxic, fast, high yield and conventional methods without high cost to synthesis nanomaterials with desired controlled size assisted with different surfactants maintained at optimum condition. The efficiency of applications merely depend on the phase purity, crystallite size and particle size

**Table 1**
Crystallite size of $CoFe_2O_4$ nanoparticles (a) $CoFe_2O_4$-CTAB (b) $CoFe_2O_4$-HMT (c) $CoFe_2O_4$-PEG.

| Sample code | Pos. [2° Th.] | FWHM Left [2° Th.] | Crystallite size (nm) |
|---|---|---|---|
| C1 (CTAB) | 35.47 | 0.2460 | 69.18 |
| C2 (HMT) | 35.48 | 0.1968 | 86.48 |
| C3 (PEG) | 35.46 | 0.1476 | 115.28 |

of the material which are easily be controlled by co-precipitation method along with sintering temperature, reaction time and other influencing processing parameters. Even though, the surfactant assisted synthesis is very common, the role of surfactant influence on the magnetic behavior investigation is quite novel. The present study also revealed that the surfactant is one of the important dominating key to tune the material morphology.

The phase and structural analysis of synthesized nanoferrites was confirmed by employing X-ray diffraction (XRD) measurements and disclosed in Fig. 1a–c. The obtained XRD results revealed the formation of face centered cubic $CoFe_2O_4$ belongs to Fd3m space group with inverse spinel structure [25]. The diffraction peaks situated at the $2\theta$ values of 30, 35, 37, 43, 57 and 62° communicate to the respective crystal planes (220), (311), (222), (400), (511) and (440) exactly harmonized with standard JCPDS no #22-1086 [25,26]. The tetrahedral A and octahedral B site of inverse spinel structure are specified by unit cell length a and the oxygen position in the unit cell. The average lattice constant calculated from XRD data is 0.833 nm and coincided with standard JCPDS card value which shows the formation of inverse spinel structure. The unit cell parameter (a) is related to the $2\theta$ peak positions. The obtained increase in intensity of (311) planes shows the appropriate presence of the position of the oxygen atoms in the unit cell. In inverse spinel structure, the divalent $Co^{2+}$ ions are located in the octahedral positions, while half of the $Fe^{3+}$ ions are situated at the tetrahedral sites and the other half at the octahedral sites. The cation sensitive planes (220) and (440) denoted the cations present in the tetrahedral A site and octahedral B site of inverse spinel ferrite system in XRD.

The crystallite size of the sample is calculated from XRD data by employing Debye–Scherrer formula: $D = 0.9\lambda/\beta \cos\theta$; where $\lambda$ denotes X-ray wavelength, $\beta$ denotes the full width at half maximum intensity and $\theta$ stands Bragg's angle. The crystallite size of first maxima (largest peak) has been calculated by using the conventional formula and found to be as 69.18, 86.48 and 115.28 nm for samples using the surfactants CTAB, HMT and PEG respectively as shown in Table 1. The sample synthesized with CTAB shows some amorphous nature compared to HMT and PEG respectively. However, the first maxima of all the three samples are well defined which revealed the good quality of formation of cobalt ferrite. The obtained crystallite size variation is likely to be more dominant in the ferrimagnetic behavior of the product. The crystallite size calculated from XRD revealed that the product synthesized using HMT and PEG-400 possessed larger crystallite size compared to C1. Owing to the basic concept of magnetism, the magnetization and demagnetization of the product mainly depend on the domain wall movements. These movements entailed minimum energy than the domains rotational energy. In view of the fact that the larger grain size promoted the number of domain walls inside the product which originates the higher energy requirement of domain wall movement for magnetization and demagnetization than the energy consumed for rotation of domains [27]. It brought the expectation of high saturation and low coercivity of the product. Therefore, the obtained results revealed that the crystalline nature and crystallite size of the samples depends on surfactants used in the processing method which influences the ferrimagnetic domain walls.

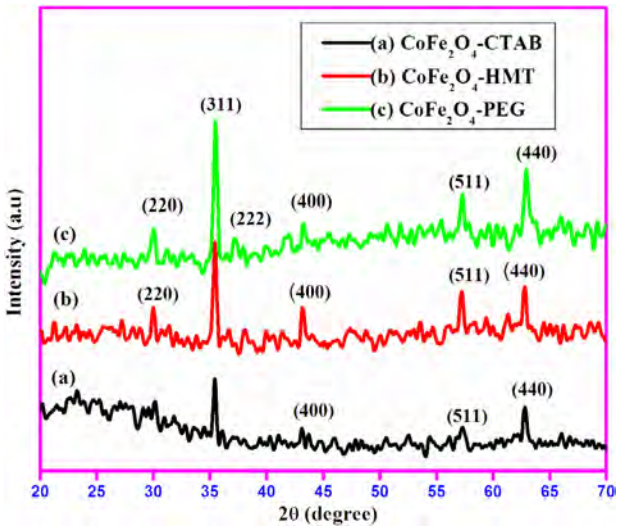


**Fig. 1.** XRD pattern of $CoFe_2O_4$ nanoparticles (a) $CoFe_2O_4$-CTAB (b) $CoFe_2O_4$-HMT (c) $CoFe_2O_4$-PEG.

Scanning electron microscope images were taken out to reveal the morphology and approximate particle size of the synthesized magnetic cobalt ferrite ($CoFe_2O_4$) nanoparticles. Fig. 2a–c exposed 1 μm scale SEM images of the product. All three samples possess spherical morphology with some agglomeration. Fig. 2a represented fine nanoparticle morphology of product using CTAB and the estimated particle range is around 90–120 nm with uniform distribution. The observed clear particle edges of the nanoferrite (Fig. 2a) with less coalescence may enhance the conductivity of the product [28]. Fig. 2b represented the morphology of product using HMT which revealed the formation of nanoparticles in the range of 100–250 nm with compact distribution. Fig. 2c showed the inhomogeneous morphology of the product using PEG with uneven diameter of the particles in the range of 200–500 nm. This kind of particle nature induces the ferrimagnetic behavior of the synthesized cobalt ferrite due to its oriented spin arrangement. SEM images of the synthesized nanoferrite samples revealed an idea about the morphology and particle size variation regarding the surfactants used in the processing method. SEM images show the particle size of the product whereas XRD calculation gives the crystallite size of the product. A particle may contain one or more than one grains. In our case, the surfactant made an impact on the particle size and nature except the shape of the sample.

The phase impurities, structural confirmation and phonon vibration modes of the obtained product are investigated through Raman studies. Fig. 3a–c illustrated the room temperature Raman spectra of cobalt ferrite ($CoFe_2O_4$) nanoparticles synthesized by employing CTAB, HMT and PEG respectively. The Raman assignments of the obtained product are shown in Table 2. It clearly exaggerated the formation of cubic cobalt ferrite nanoparticles. Three Raman active modes such as $E_g$, $T_{1g}(1)$ and $A_{1g}(1)$ respectively at ~280, ~535 and ~673 $cm^{-1}$ are identified for the product C1. Moreover, four Raman active modes such as $E_g$, $T_{1g}(1)$, $T_{1g}(2)$ and $A_{1g}(1)$ for the product C2 and C3 is respectively located at ~285, ~465, ~570 and ~675 $cm^{-1}$. These bands are closely matched with literally reported phonon vibration modes of ferrimagnetic cobalt ferrite ($CoFe_2O_4$) nanoparticles. Further, the synthesized cobalt ferrite nanoparticles are in perfect inverse spinel structure with typical room temperature ferrimagnetic behavior evidenced by noticing the same $A_{1g}(1)$ intensity vibration mode. The observed results revealed that the surfactant used in the processing technique never change the inverse structure of the ferrite system [29].

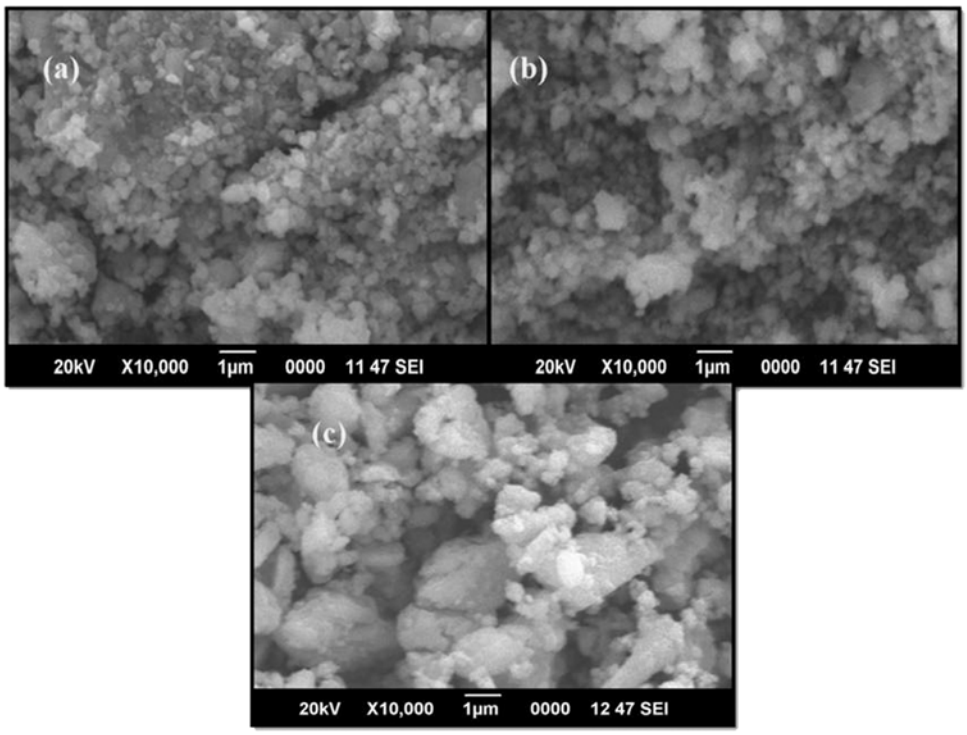


**Fig. 2.** SEM images of $CoFe_2O_4$ nanoparticles (a) $CoFe_2O_4$-CTAB (b) $CoFe_2O_4$-HMT (c) $CoFe_2O_4$-PEG.

**Table 2**
Raman modes of $CoFe_2O_4$ nanoparticles (a) $CoFe_2O_4$-CTAB (b) $CoFe_2O_4$-HMT (c) $CoFe_2O_4$-PEG.

| Assignment) | $E_g$ | $T_{1g}(1)$ | $T_{1g}(2)$ | $A_{1g}(1)$ |
|---|---|---|---|---|
| | ($cm^{-1}$) | | | |
| C1 | ∼280 | ∼535 | – | ∼673 |
| C2 | ∼285 | ∼465 | ∼570 | ∼675 |
| C3 | ∼285 | ∼465 | ∼570 | ∼675 |

The line broadening of the sample with small grain size mainly caused by the scattering of phonon due to the increase of point defect and abundant surface atoms which led to the presence of more hanging bonds and metal oxygen chain deformation [30]. In the present study, the same line broadening effect is also observed for the cobalt ferrite sample synthesized using CTAB which is also reflected in the ferrimagnetic magnetic behavior of the product as shown in VSM studies. Raman spectra of cobalt ferrite ($CoFe_2O_4$) showed the influence of the surfactant used in the protocol by directing the particle size of the samples conclusively.

The photoluminescence study was carried out to examine the electronic transition, point defect, luminescent behavior and optical properties of the synthesized cobalt ferrite ($CoFe_2O_4$) nanoparticles. The emission peaks are observed in the range between UV to visible region by exciting the wavelength by 320 nm (Fig. 4a–c). While exciting the material, electrons excitation by the absorption of phonons and the excitons return to the ground state results the occurrence of emission peaks in PL spectra depending on the surface oxides, size and surface defect etc. According to ferrimagnetic ferrite systems, the charge transfer mechanism between trivalent ions majorly concern the non-radiative super exchange process due to intervening oxide ions which led to magnetic ordering of the domains in the material [31]. The obtained PL spectrum revealed the visible range intrinsic and extrinsic bands of cobalt ferrite. Four high intense strong emission peaks and two lower intense peaks were found. The peaks located at 361, 378 and 393 nm represented

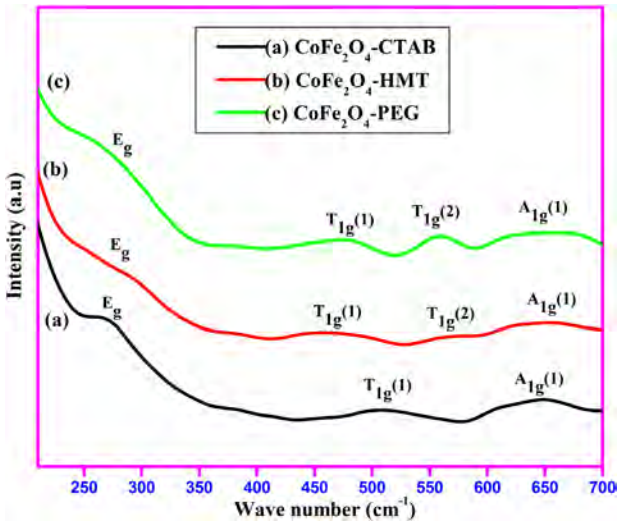


**Fig. 3.** Raman spectra of $CoFe_2O_4$ nanoparticles (a) $CoFe_2O_4$-CTAB (b) $CoFe_2O_4$-HMT (c) $CoFe_2O_4$-PEG.

the near band edge emission of nano sized materials. The moderately high intense visible bands observed at 408 nm could be attributed to the intrinsic defects which include interstitial cobalt and iron defects. The predominant peak observed at 419 nm could be attributed to the recombination of electrons intensely trapped with photo-generated holes in oxygen vacancies [32]. The final emission peak located at nearly 460 nm could be attributed to $3d^5 \rightarrow 3d^4$ 4s transitions of $Fe^{+3}$ ions in ferrite system. In this transition, an excited electron in the conduction band balanced the 4s orbital of $Fe^{3+}$ from the localized $3d^5$ state of $Fe^{3+}$. In our case, the slight variation of intensity was found for the samples with the variation of surfactants. The smaller particles size cobalt ferrite (C1) showed high intense luminous spectra compared to

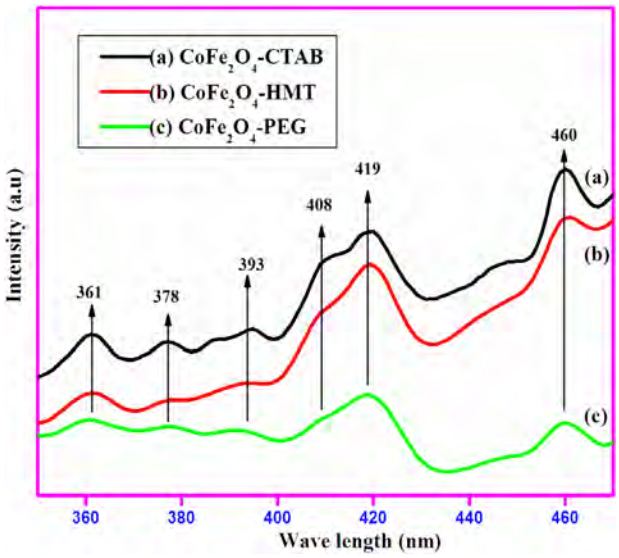


**Fig. 4.** PL spectra of $CoFe_2O_4$ nanoparticles (a) $CoFe_2O_4$-CTAB (b) $CoFe_2O_4$-HMT (c) $CoFe_2O_4$-PEG.

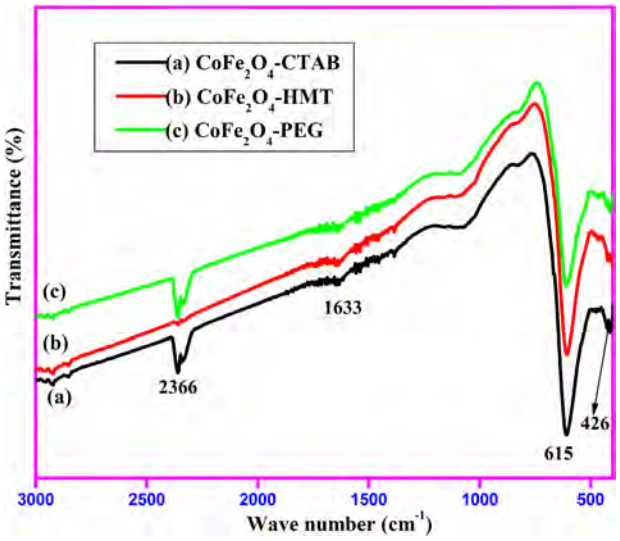


**Fig. 5.** FTIR spectra of $CoFe_2O_4$ nanoparticles (a) $CoFe_2O_4$-CTAB (b) $CoFe_2O_4$-HMT (c) $CoFe_2O_4$-PEG.

other samples due to the decreasing non-radiative contribution with decreased particle and large number of particles per unit area facing towards the incident light [33]. This kind of high luminescent behavior of the small grain sized cobalt ferrite product possess less ferrimagnetic behavior compared to the sample with low luminescent property due to large grain size. Due to the small particle size with high spin canting, the fluorescence intensity enhances and reduces the saturation magnetization of the ferrimagnetic cobalt ferrite. Hence, the surfactant variations highly affected the photoluminescence properties of nanoferrites.

The metal oxygen vibration modes present in the tetrahedral and octahedral sites of ferrite system is further confirmed employing FTIR spectra. Fig. 5a–c represented the corresponding metal oxygen vibrations and functional groups present in the magnetic cobalt ferrite nanoparticles. The strong signature observed at 2366 $cm^{-1}$ is assigned to the adsorption of atmospheric $CO_2$. The disturbances in absorption band in between the range 1500–1600 $cm^{-1}$ is assigned to N=O stretching vibration. A broad envelope present near the wave number 1000 $cm^{-1}$ is assigned to the nitrate ion traces. A well-built absorption band observed at 615 $cm^{-1}$ is attributed to the octahedral cation group complex ($Co^{2+}$-$O^{2-}$) vibration mode of cobalt ferrite nanoparticles [34]. An accountable absorption band observed at 426 $cm^{-1}$ is attributed to the tetrahedral cation ($Fe^{3+}$-$O^{2-}$) vibration mode of synthesized cobalt ferrite nanoparticles [35]. No noteworthy changes are observed in finger print region for all the three samples.

The electrochemical behavior of the cobalt ferrite material is analyzed by employing cyclic voltammetry (CV) study (Fig. 6a–c) and explored the investigation on electrochemical characterization of $CoFe_2O_4$ as an active material on the low cost graphite sheet chosen as charge collector. The specific capacitance of the product depends on the scan rate of cyclic voltammetry. As the scan rate increases, the specific capacitance of the material decreases which merely due to the minimal utilization of availing active sites of working electrode by the electrolyte ions. The cyclic voltammogram curve of synthesized cobalt ferrite nanoparticles in 1 M NaOH electrolyte solution and the specific capacitance versus scan rate relation are shown in Fig. 6a–d. CV curves explain the pseudocapacitive behavior of cobalt ferrite through the well defined redox peak. The scan rate is increased as 25, 50, 75 and 100 mV/s to map out the CV curve. The adopted formula for calculating specific capacitance

**Table 3**
Calculated specific capacitance values for different scan rates at 15, 30, 45 and 60 mV/s of $CoFe_2O_4$ nanoparticles (a) $CoFe_2O_4$-CTAB (b) $CoFe_2O_4$-HMT (c) $CoFe_2O_4$-PEG.

| Sample code | Specific capacitance value (F/g) | | | |
|---|---|---|---|---|
| | Scan rate (mV/s) | | | |
| | 15 | 30 | 45 | 60 |
| C1 | 178.33 | 120.13 | 119.24 | 114.06 |
| C2 | 155.72 | 114.52 | 93.87 | 71.29 |
| C3 | 99.67 | 87.78 | 72.72 | 63.47 |

was given by $C = I(V)dV/\Delta m \times S \times (V_2 - V_1)|_{V_1 \text{ to } V_2}$, where $(I(V)dV)$ is the area of CV curve, $(\Delta m)$ the mass of the active material layered on the graphite substrate, $(S)$ the scan rate value and $(V_2 - V_1)$ the potential window difference. The values of calculated specific capacitance are tabularized for all the three samples for different scan rates (25, 50, 75 and 100 mV/s) respectively. The pesudocapacitive mechanism of cobalt ferrite mainly depends on the electrochemical adsorption–desorption reaction at the interface between electrode and electrolyte [34]. The redox reactions of cobalt ferrite are indicated by the reaction $Co^{II} \leftrightarrow Co^0$ and $Fe^{III} \leftrightarrow Fe^0$ [36]. The calculated specific capacitance values for cobalt ferrite synthesized by using CTAB, HMT and PEG are 178.33, 155.72 and 99.67 F/g respectively at 15 mV/s. From the keen observation of Table 3, the cobalt ferrite sample assisted CTAB with smaller crystallite and particle size shows the high specific capacitance value. Fig. 6 clearly revealed that the redox peak and the area under the peak are curves out to be small for the samples synthesized using surfactants HMT and PEG compared to the sample synthesized using CTAB, i.e., cobalt ferrite with particle size ~90–120 nm showed the high redox current due to the increase of active surface taken into account during electrode/electrolyte reaction [37]. Hence, the surfactants used in the synthesis process played an inevitable role in the electrochemical behavior of the nanoferrite material. The cobalt ferrite sample synthesized by using CTAB surfactant showed the lower crystalline nature which cause for higher conductivity of the sample may possess high specific capacitance value evidenced by CV studies.

The magnetic properties of cobalt ferrite ($CoFe_2O_4$) with varying crystallite size kindled the great insight of nanomaterial's magnetic behavior. Room temperature vibrating sample magnetometer was carried out with applied field ranging from −2 to +2 tesla (1 tesla

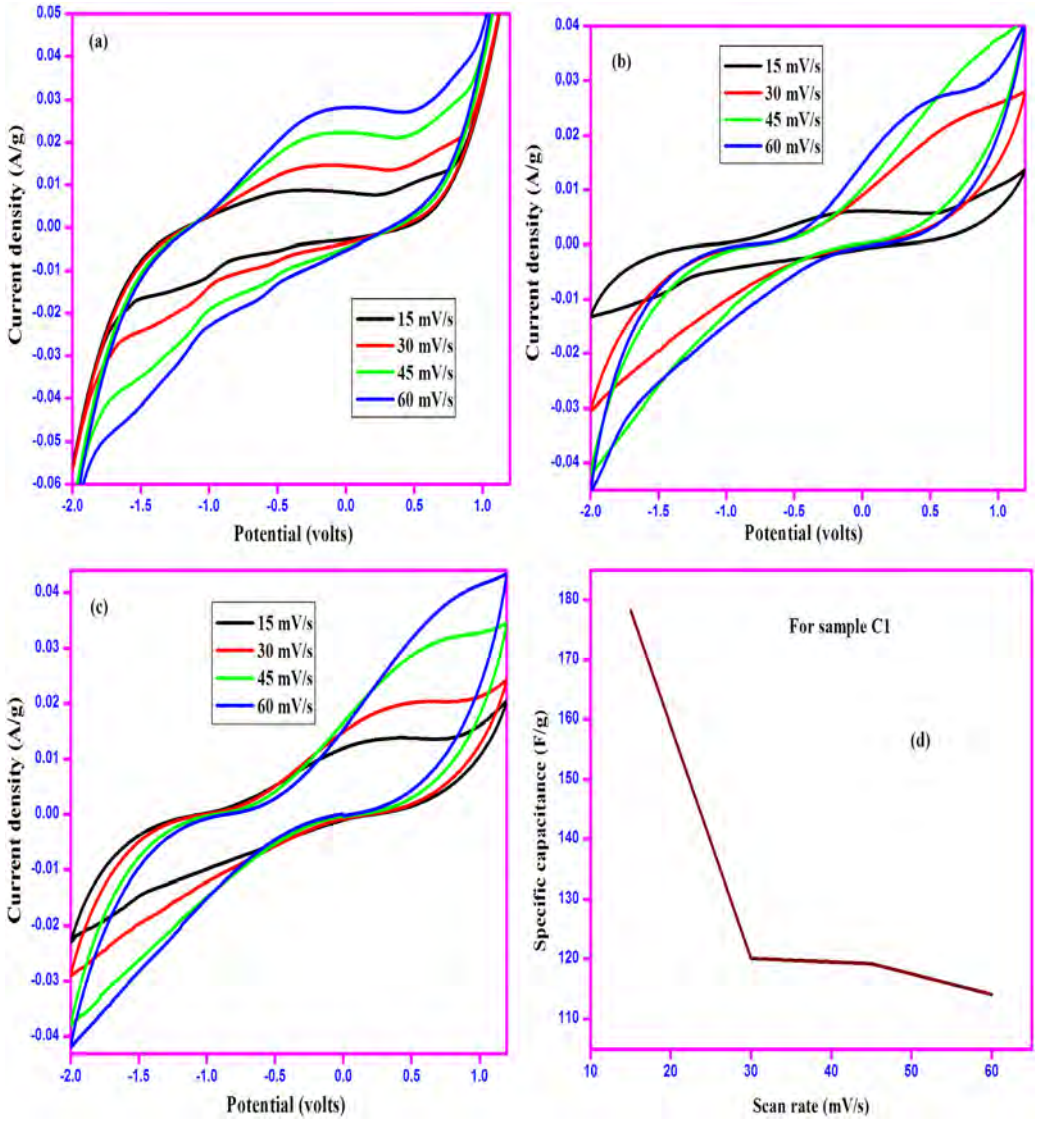


**Fig. 6.** CV studies of $CoFe_2O_4$ nanoparticles (a) $CoFe_2O_4$-CTAB (b) $CoFe_2O_4$-HMT (c) $CoFe_2O_4$-PEG (d) Relationship between scan rate vs. specific capacitance.

**Table 4**
Saturation magnetization, remanent magnetization and coercivity value of $CoFe_2O_4$ nanoparticles (a) $CoFe_2O_4$-CTAB (b) $CoFe_2O_4$-HMT (c) $CoFe_2O_4$-PEG.

| Sample code | Crystallite size (nm) | Saturation magnetization ($M_s$) | Remanent magnetization ($M_r$) | Coercivity value (Oe) | Remanence ratio ($M_r/M_s$) |
|---|---|---|---|---|---|
| C1 | 69.18 | 58.8 | 42.5 | 803 | 0.72 |
| C2 | 86.48 | 61.9 | 46.0 | 802 | 0.74 |
| C3 | 115.28 | 66.0 | 48.0 | 801 | 0.73 |

$= 10^4$ Oe). Fig. 7a–c demonstrated the ferrimagnetic hysteresis loop of synthesized cobalt ferrite ($CoFe_2O_4$) by using CTAB, HMT and PEG respectively. Plenty of factors may affect the magnetic behavior of the nanomaterials in which crystallite and particle size and shape played a dominant role. All the three samples exhibited the room temperature ferrimagnetism with different saturation, remanent and coercive value. VSM results of maximum saturation magnetization ($M_s$), coercivity ($H_c$), remanent magnetization ($M_r$) and remanence ratio values for each sample is shown in Table 4. The saturation magnetization values for the samples C1, C2 and C3 are 58.8, 61.9 and 66 emu/g, the remanent magnetization are 42.5, 46 and 48 emu/g respectively. The overall low coercive value and its negligible difference found to be 803, 802 and 801 Oe for the respective samples C1, C2 and C3 is due to the motion of the walls [38]. The calculated remanence ratio of the products C1, C2 and C3 are 0.72, 0.74 and 0.73 respectively which directly proportional to the crystallite size of the product [39]. According to the result, the visible increment in the maximum saturation magnetization and maximum remanent was observed for the sample synthesized using the surfactant PEG whose approximate particle size was high (200–500 nm) compared to other samples synthesized by using CTAB and HMT. It obviously showed that the increase in particle size provided the increased saturation magnetization mainly attributed to the lower surface spin canting and lower surface disorder of the cobalt ferrite sample [40]. From Fig. 7, the high saturation magnetization of about 66 emu/g was observed for C3 sample. As the particle size increases, the ferrimagnetization also gets increased in the present study.

The same trend of improved ferrimagnetization of the product with large particle and crystallite size was observed in the present study. This noticeable increment in saturation magnetization may due to high ordered spin arrangement of spinel ferrite. The smaller

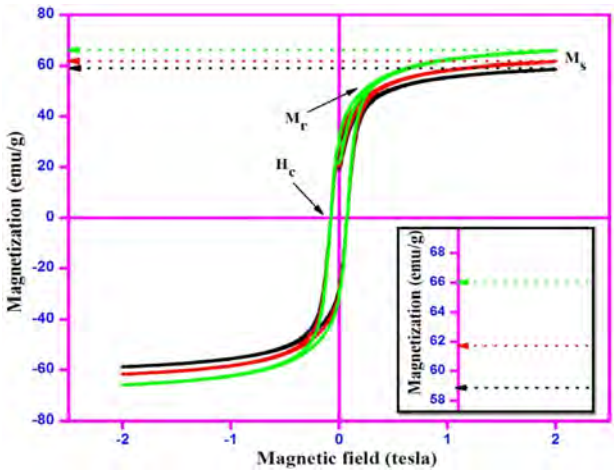


**Fig. 7.** M–H loop of synthesized $CoFe_2O_4$ nanoparticles (a) $CoFe_2O_4$-CTAB (b) $CoFe_2O_4$-HMT (c) $CoFe_2O_4$-PEG.

values of saturation magnetization observed for the samples with smaller crystallite size may due to the irregularity of spin and the presence of spin slanting inside the material [41]. The overall decrease in saturation magnetization observed than bulk cobalt ferrite whose value is 73 emu/g may be ascribed to the surface effects stimulated by the magnetic moment distortion at the surface of the nanocrystallites. Literature report explored that the particles with larger particle size than that of single crystal domain (34 nm) size contained multi domain nanocrystallites [41]. In the present study, the size of all particles were much larger than single crystal domain size capitulated the less coherent spin rotation and predominance of domain wall formation in ferrimagnetic cobalt ferrite product [39]. The asymmetric nature observed in the magnetization values ($M_s$) may be due to the involvement of non uniform resonance of the samples in addition to the main resonance mode of the sample [42]. Moreover, this asymmetric nature may also be due to the inhomogeneous particle size of the three samples. VSM results clearly revealed that both the crystallite and particle size played a significant role in deciding the ferrimagnetic properties of cobalt ferrite nanoparticles. One of the controlling parameters for manipulating the particle and crystallite size is choosing a suitable surfactant used in synthesis protocol which definitely tune the room temperature ferrimagnetic behavior of the synthesized cobalt ferrite product proven by VSM study. All the evidences showed that the surfactant variation presumably influenced the physico-chemical and magnetic properties of cobalt ferrite nanoparticles.

## 4. Conclusions

The physico-chemical and magnetic properties of cobalt ferrite via simple co-precipitation route using the surfactants CTAB, HMT and PEG was investigated. XRD results revealed the cubic face centered spinel structure. SEM images revealed the spherical morphology with uneven particle sizes. A well defined Raman active mode with surfactant corresponding shift was revealed by Raman spectra. The luminescent property purely depends on particle size of the products. The strong metal oxygen signature was confirmed for all the three samples. The highest specific capacitance was observed for the sample synthesized by using CTAB which revealed that the nano sized materials are always capable of possessing high specific capacitance. The room temperature ferrimagnetism was observed for the sample synthesized by using the surfactant PEG-400 due to its larger particle size. These results elucidated that the surfactants used in the product processing method is an important tool to control the properties of nanoferrites.

## Acknowledgment

This work was supported by UGC Start-Up Research Grant No. F.30-326/2016 (BSR).

## References

[1] A. Hajaliloua, S.A. Mazlana, M. Abbasib, H. Lavvafi, Fabrication of spherical $CoFe_2O_4$ nanoparticles with a sol–gel and hydrothermal methods and investigation their magnetorheological characteristics, RSC Adv. 6 (2016) 89510–89522.
[2] S.C. Goh, C.H. Chia, S. Zakaria, M. Yusoff, C.Y. Haw, Sh. Ahmadi, N.M. Huang, H.N. Lim, Hydrothermal preparation of high saturation magnetization and coercivity cobalt ferrite nanocrystals without subsequent calcinations, Mater. Chem. Phys. 120 (2010) 31–35.
[3] D. Alonso-Domínguez, M.L. López, L. García-Quintana, I. Álvarez Serrano, C. Pico, M.L. Veiga, Lithium-ion full cell battery with spinel-type nanostructured electrodes, Nano-Struct. Nano-Objects 11 (2017) 88–93.
[4] C. Colombo, G. Palumbo, E.D. Iorio, X. Song, Z. Jiang, Q. Liu, R. Angelico, Influence of hydrothermal synthesis conditions on size, morphology and colloidal properties of Hematite nanoparticles, Nano-Struct. Nano-Objects 2 (2015) 19–27.
[5] R. Safi, A. Ghasemi, R.S. Razavi, M. Tavousi, The role of pH on the particle size and magnetic consequence of cobalt ferrite, J. Magn. Magn. Mater. 396 (2015) 288–294.
[6] D. Khallafallah Hassen, M.M. Selim, S.A. El-Safty, Khalil Abdelrazek Khalil, G. Abuel-Maged, M. Dewidar, Graphene-supported $Co(OH)_2$ mesostructures for ethanol oxidation reaction electrocatalysis, Nano-Struct. Nano-Objects 9 (2017) 31–39.
[7] N.V. Long, Y. Yang, T. Teranishi, C.M. Thi, Y. Cao, M. Nogami, Synthesis and magnetism of hierarchical iron oxide particles, Mater. Des. 86 (2015) 797–808.
[8] M. Sedlacik, V. Pavlinek, P. Peerd, P. Filip, Tailoring the magnetic properties and magnetorheological behavior of spinel nanocrystalline cobalt ferrite by varying annealing temperature, Dalton Trans. 43 (2014) 6919.
[9] Nguyen Viet Long, Yong Yang, Toshiharu Teranishi, Cao Minh Thi, Yanqin Cao, Masayuki Nogami, Biomedical applications of advanced multifunctional magnetic nanoparticles, J. Nanosci. Nanotechnol. 15 (2015) 10091–10107.
[10] Venkata Manthinaa, Alexander G. Agrios, Single-pot ZnO nanostructure synthesis by chemical bath deposition and their applications, Nano-Struct. Nano-Objects 7 (2016) 1–11.
[11] I. Aritana Fernandes de Medeiros, A. Luis Lopes-Moriyama, C. Pereira de Souza, Effect of synthesis parameters on the size of cobalt ferrite crystallite, Ceram. Int. 43 (2017) 3962–3969.
[12] N.V. Long, Y. Yang, T. Teranishi, C. Minh Thi, Y. Cao, M. Nogami, Synthesis and related magnetic properties of $CoFe_2O_4$ cobalt ferrite particles by polyol method with $NaBH_4$ and heat treatment: New micro and nanoscale structures, RSC Adv. 5 (70) (2015) 56560–56569.
[13] A. Sundararaj, G. Chandrasekaran, Induced phase transition from ZnO to $Co_3O_4$ through Co substitution, Nano-Struct. Nano-Objects 11 (2017) 20–24.
[14] M.A. Gabal, A.A. Al-Juaid, S.M. Al-Rashed, M.A. Hussein, F. Al-Marzouki, PSynthesis, characterization and electromagnetic properties of Zn-substituted $CoFe_2O_4$ via sucrose assisted combustion route, J. Magn. Magn. Mater. 426 (2017) 670–679.
[15] B. Pourgolmohammad, S.M. Masoudpanah, M.R. Aboutalebi, Effect of starting solution acidity on the characteristics of $CoFe_2O_4$ powders prepared by solution combustion synthesis, J. Magn. Magn. Mater. 424 (2017) 352–358.
[16] S. Fatemeh Shams, M. Kashefi, C. Schmitz-Antoniak, Statistical approach of synthesize $CoFe_2O_4$ nanoparticles to optimize their characteristics using response surface methodology, J. Magn. Magn. Mater. 432 (2017) 362–372.
[17] S. Joshi, M. Kumar, S. Chhoker, A. Kumar, M. Singh, Effect of $Gd^{3+}$ substitution on structural, magnetic, dielectric and optical properties of nanocrystalline $CoFe_2O_4$, J. Magn. Magn. Mater. 426 (2017) 252–263.
[18] N. Kannapiran, A. Muthusamy, P. Chitra, S. Anand, R. Jayaprakash, Poly(o phenylenediamine)/$NiCoFe_2O_4$ nanocomposites: Synthesis, characterization, magnetic and dielectric properties, J. Magn. Magn. Mater. 423 (2017) 208–216.
[19] M. Kishimoto, H. Latiff, E. Kita, H. Yanagihara, Characterization of FeCo particles synthesized via co-precipitation, particle growth using flux treatment and reduction in hydrogen gas, J. Magn. Magn. Mater. 432 (2017) 404–409.
[20] K. Ali, A. Bahadur, A. Jabbar, S. Iqbal, I. Ahmad, M. Imran Bashir, Synthesis, structural, dielectric and magnetic properties of $CuFe_2O_4/MnO_2$ nanocomposites, J. Magn. Magn. Mater. 434 (2017) 30–36.
[21] R.N. Bhowmik, A.K. Sinha, Improvement of room temperature electric polarization and ferrimagnetic properties of $Co_{1.25}Fe_{1.75}O_4$ ferrite by heat treatment, J. Magn. Magn. Mater. 421 (2017) 120–131.
[22] S.V. Vijayasundaram, G. Suresh, R. Kanagadurai, Chemically synthesized phase-pure $BiFeO_3$ nanoparticles: Influence of agents on the purity, Nano-Struct. Nano-Objects 8 (2016) 1–6.

[23] C. Dey, K. Baishya, A. Ghosh, M. Mandal Goswami, A. Ghosh, K. Mandal, Improvement of drug delivery by hyperthermia treatment using magnetic cubic cobalt ferrite nanoparticles, J. Magn. Magn. Mater. 427 (2017) 168–174.
[24] C. Yang, J. Jiang, X. Liu, C. Yin, C. Deng, Rare earth ions doped polyaniline/cobalt ferrite nanocomposites via a novel coordination-oxidative polymerization-hydrothermal route: Preparation and microwave-absorbing properties, J. Magn. Magn. Mater. 404 (2016) 45–52.
[25] Z. Gu, X. Xiang, G. Fan, F. Li, Facile synthesis and characterization of cobalt ferrite nanocrystals via a simple reduction-oxidation route, J. Phys. Chem. C 112 (2008) 18459–18466.
[26] M. Vadivel, R. Ramesh Babu, K. Ramamurthi, M. Arivanandhan, Effect of PVP concentrations on the structural, morphological, dielectric and magnetic properties of $CoFe_2O_4$ magnetic nanoparticles, Nano-Struct. Nano-Objects 11 (2017) 112–123.
[27] A.C.F.M. Costa, E. Tortella, M.R. Morelli, R.H.G.A. Kiminami, Synthesis, microstructure and magnetic properties of Ni–Zn ferrites, J. Magn. Magn. Mater. 256 (2003) 174–182.
[28] A. Mohammad Toufiq, F. Wang, Q.U. Ain Javed, Q. Li, Y. Li, M. Khan, Synthesis, characterization and photoluminescent properties of 3D nanostructures self-assembled with $Mn_3O_4$ nanoparticles, Mater. Express 4 (2014) 3.
[29] P. Chandramohan, M.P. Srinivasan, S. Velmurugan, S.V. Narasimhan, Cation distribution and particle size effect on Raman spectrum of $CoFe_2O_4$, J. Solid State Chem. 184 (2011) 89–96.
[30] L. Li, Z. Hu, Y. Yang, P. Liang, A. Lu, H. Xu, Y. Hu, H. Wu, Hydrothermal self-assembly synthesis of $Mn_3O_4$/reduced graphene oxide hydrogel and its high electrochemical performance for supercapacitors, Chin. J. Chem. 31 (2013) 1290–1298.
[31] R.K. Singh, A. Narayan, K. Prasad, R.S. Yadav, A.C. Pandey, A.K. Singh, L. Verma, R.K. Verma, Thermal, structural, magnetic and photoluminescence studies on cobalt ferrite nanoparticles obtained by citrate precursor method, J. Therm. Anal. Calorim. 110 (2012) 573–580.
[32] A. Manikandan, M. Durka, K. Seevakan, S. Arul Antony, A novel one-pot combustion synthesis and opto-magnetic properties of magnetically separable spinel $Mn_xMg_{1-x}Fe_2O_4$ ($0.0 \leq x \leq 0.5$) nanophotocatalysts, J. Supercond. Novel Magn. 28 (2015) 1405–1416.
[33] P.K. Sharma, M.H. Jilavi, R. Nass, H. Schmidt, Tailoring the particle size from $\mu$m $\rightarrow$ nm scale by using a surface modifier and their size e!ect on the fluorescence properties of europium doped yttria, J. Lumin. 82 (1999) 187–193.
[34] V.S. Kumbhar, A.D. Jagadale, N.M. Shinde, C.D. Lokhande, Chemical synthesis of spinel cobalt ferrite (CoFe2O4) nano-flakes for supercapacitor application, Appl. Surf. Sci. 259 (2012) 39–43.
[35] L. Zhaoa, H. Zhanga, Y. Xinga, S. Songa, S. Yua, W. Shia, X. Guoa, J. Yanga, Y. Leia, F. Cao, Studies on the magnetism of cobalt ferrite nanocrystals synthesized by hydrothermal method, J. Solid State Chem. 181 (2008) 245–252.
[36] Y.Q. Chu, Z.W. Fu, Q.Z. Qin, Cobalt ferrite thin films as anode material for lithium ion batteries, Electrochim. Acta 49 (2004) 4915–4921.
[37] H. Karami, B. Kafi, S. Najmmadin Mortazavi, Effect of particle size on the cyclic voltammetry parameters of nanostructured lead dioxide, Int. J. Electrochem. Sci. 4 (2009) 414–424.
[38] D.L. Leslie-Pelecky, R.D. Rieke, Magnetic properties of nanostructured materials, Chem. Mater. 8 (1996) 1770.
[39] Y. Qu, H. Yang, N. Yang, Y. Fan, H. Zhu, G. Zou, The effect of reaction temperature on the particle size, structure and magnetic properties of coprecipitated CoFe2O4 nanoparticles, Mater. Lett. 60 (2006) 3548–3552.
[40] T. Sodaee, A. Ghasemi, R. Shoja Razavi, Controlled growth of large-area arrays of gadolinium-substituted cobalt ferrite nanorods by hydrothermal processing without use of any template, Ceram. Int. 42 (2016) 17420–17428.
[41] A. Amirabadizadeh, Z. Salighe, R. Sarhaddi, Z. Lotfollahi, Synthesis of ferrofluids based on cobalt ferrite nanoparticles: Influence of reaction time on structural, morphological and magnetic properties, J. Magn. Magn. Mater. 434 (2017) 78–85.
[42] B. Parvatheeswara Rao, C.O. Kim, C.G. Kim, I. Dumitru, L. Spinu, O.F. Caltun, Structural and magnetic characterizations of coprecipitated Ni-Zn and Mn-Zn ferrite nanoparticles, IEEE Trans. Magn. 42 (2006) 10.